Inelastic buckling strength of stiffened plates in compression

Inelastic Buckling Strength of Stiffened Plates in Compression

Résistance au voilement, dans le domaine inélastique, de tôles raidies comprimées

Traglast längsversteifter und gedrückter Bleche im unelastischen Beulbereich

Yuhshi FUKUMOTO

Professor of Civil Engineering
Nagoya University
Nagoya, Japan

Tsutomu USAMI

Assistant Professor of Structural Engineering
Asian Institute of Technology
Bangkok, Thailand

Koichiro YAMAGUCHI

Graduate Student
Nagoya University
Nagoya, Japan

SUMMARY

A theoretical and experimental investigation is presented on the strength of longitudinally stiffened steel plate in edge compression. The stiffened plates treated in this paper are of relatively low width-thickness ratios and of relatively rigid stiffeners. From the numerical study it has been found out that the strength of such stiffened plates is reduced considerably by early yielding in the stiffeners caused by welding residual stresses. A comparison between the calculated buckling strengths and the experimental maximum loads has shown that the prediction is generally in reasonably good agreement with the test results.

RÉSUMÉ

L'article présente une étude théorique et expérimentale sur la résistance de tôles métalliques comprimées munies de raidisseurs longitudinaux. Les tôles raidies — considérées dans l'article — présentent des rapports largeur/épaisseur relativement bas et ont des raidisseurs relativement rigides. Les résultats numériques montrent que la résistance de telles tôles raidies est réduite considérablement par un écoulement précoce provoqué par les contraintes résiduelles de soudure dans les raidisseurs.

Une comparaison entre les résistances au voilement, calculées, et les charges expérimentales de rupture, montrent une bonne correspondance entre la théorie et les essais.

ZUSAMMENFASSUNG

Die Autoren bringen theoretische und experimentelle Untersuchungen vor über die Traglast längsversteifter und längsgedrückter Stahlbleche. Die Schlankheit, d.h. das Verhältnis Breite/Dicke, der untersuchten längsversteiften Bleche ist relativ klein und die Längsrippen sind relativ steif. Die Berechnungsergebnisse zeigen, dass ein frühzeitiges, durch die Schweisseigenspannung bedingtes Fliessen der Steifen die Traglast solcher versteifter Bleche erheblich vermindert. Die Übereinstimmung zwischen den rechnerisch ermittelten Traglasten und den experimentellen Werten ist gut.

1. INTRODUCTION

Recently, a number of investigations have been published on the strength of longitudinally and/or transversely stiffened steel plates in compression [6]. Most of the studies are concerned with the strength and design of stiffened plates used as compression flanges of steel box girders. Such stiffened plates usually have relatively large width-thickness ratios, and thus the effects of initial geometrical imperfections and post-buckling strength have been the major subjects to be discussed. However, in the case of relatively thick stiffened plates, such as component plates of suspension bridge towers, welding residual stresses will have more pronounced influence on their ultimate strength than geometric imperfections, because those plates have high buckling strengths and therefore loss of the effective flexural rigidity of the stiffeners becomes considerable due to early yielding in the stiffeners. The present study is concerned with the strength of such stiffened plates. It has been pointed out [16] that unstiffened plates with low width-thickness ratios reserve little post-buckling strength and, therefore, the ultimate and buckling strengths are for all practical purposes identical. This idea is extended into stiffened plates and their compressive strengths are determined in this paper from an elastic-plastic buckling theory with residual stresses taken into consideration. In order to substantiate the theoretical results, a total of twenty-seven failure tests were performed using simply supported plates with three to five equidistant longitudinal stiffeners of flat type. In addition to the failure tests, residual stress distributions were measured on six plates with stiffeners of various dimensions.

2. THEORY

2.1 Method of Numerical Analysis

Figure 1 shows a stiffened plate to be analyzed. The plate is simply supported along the four edges and subjected to uniform edge compression σ. The stiffeners are of either a flat or a tee section, and divide the plate into n equal subpanels. The problem will be analyzed by means of the finite strip method [7,17]. Fundamental assumptions made in the analysis are: (1) the material has an elastic-perfectly plastic stress-strain relationship, (2) neigher out-of-flatness nor out of straightness exists in the plate and its stiffeners prior of buckling, (3) residual normal stresses in the direction of loading are locked in as shown in Fig. 2, and (4) no strain reversal takes place at the instant of buckling and the deformation theory of Bijlaard [1,15] is valid in the plastic range, and (5) the cross-sectional dimensions of stiffeners are all the same in a stiffened plate. The residual stress patterns in Fig. 2 were so determined that the self-equilibrating conditions were satisfied independently within each plate subpanel and within each stiffener. The assumed residual stress patterns will be compared with measured distributions in the subsequent section. Now, let the plate panel be divided into a number of strips. The element force-displacement equation will be first derived for a typical plate strip ij (Fig. 1). The total potential energy Π of the strip element ij just after buckling is given by

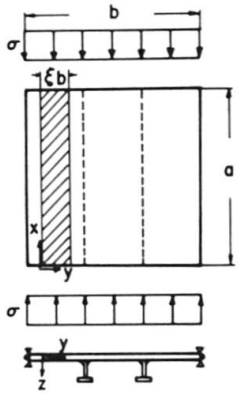

Fig. 1 Stiffened Plate to be Analysed

$$\Pi = \frac{1}{2}\int_0^a\int_0^{\xi b}\{\kappa\}^T[D]\{\kappa\}dxdy - \frac{t}{2}\int_0^a\int_0^{\xi b}\sigma\left(\frac{\partial w}{\partial x}\right)^2 dxdy - \int_0^a\{q\}^T\{Q\}dx \qquad (1)$$

where w = normal plate deflection, t = thickness of plate, b = total width of the stiffened plate, ξb = width of the plate strip,

$$\{\kappa\}^T = \left\lfloor -\frac{\partial^2 w}{\partial x^2} \; , \; -\frac{\partial^2 w}{\partial y^2} \; , \; 2\frac{\partial^2 w}{\partial x \partial y} \right\rfloor ,$$

$$\{q\}^T = \left\lfloor \frac{w_i}{b} \; , \; \theta_i \; , \; \frac{w_j}{b} \; , \; \theta_j \right\rfloor , \qquad (2)$$

$$\{Q\}^T = \left\lfloor v_i b \; , \; M_i \; , \; v_j b \; , \; M_j \right\rfloor$$

Here, w_i, θ_i, w_j and θ_j denote the deflection and slope along nodal lines i and j, respectively, and V_i, M_i, V_j and M_j represent the total shearing force and bending moment along nodal lines i and j, respectively. Matrix [D] represents the flexural rigidity matrix of the strip, which is expressed as

$$[D] = D \begin{bmatrix} d_1 & d_2 & 0 \\ d_2 & d_3 & 0 \\ 0 & 0 & d_4 \end{bmatrix} , \quad D = \frac{Et^3}{12(1-\nu^2)} \qquad (3)$$

where E = modulus of elasticity and ν = Poisson's ratio. The coefficients d_1 to d_4 are dependent on the state of stress just prior to buckling; when the stress is in the elastic range

$$d_1 = d_3 = 1.0 \; , \; d_2 = \nu \; , \; d_3 = (1-\nu)/2 \qquad (4)$$

and when the stress is in the plastic range

$$d_1 = \frac{1-\nu^2}{5-4\nu+3e} \; , \; d_2 = 2d_1 \; , \; d_3 = 4d_1 \; , \; d_4 = \frac{1-\nu^2}{2(1+\nu)+3e} \qquad (5)$$

where $e = |\varepsilon^P/\varepsilon_Y|$, ε^P = plastic component of normal strain in the direction of loading (x-axis) and ε_Y = yield strain. The normal deflection w of the strip is assumed to take the form

$$\frac{w}{b} = \lfloor N \rfloor \{\bar{q}\} \sin\frac{\pi x}{a} \; , \quad \{\bar{q}\}^T = \left\lfloor \frac{\bar{w}_i}{b} \; , \; \bar{\theta}_i \; , \; \frac{\bar{w}_j}{b} \; , \; \bar{\theta}_j \right\rfloor$$

$$\lfloor N \rfloor = \left\lfloor 1-3\bar{y}^2+2\bar{y}^3 \; , \; \xi(\bar{y}-2\bar{y}^2+\bar{y}^3) \; , \; \bar{y}^2(3-2\bar{y}) \; , \; \xi(-\bar{y}^2+\bar{y}^3) \right\rfloor \qquad (6a\text{-}c)$$

where $\bar{y} = y/\xi b$. The quantities $\bar{w}_i, \bar{\theta}_i, \bar{w}_j$ and $\bar{\theta}_j$ in Eq. (6b) are the amplitudes of the nodal line displacements w_i, θ_i, w_j and θ_j, respectively. The nodal line forces that are consistent with the assumed deflection function may be expressed in terms of their amplitudes as follows:

$$\{Q\}^T = \{\bar{Q}\}^T \sin\frac{\pi x}{a} \; , \quad \{\bar{Q}\}^T = \left\lfloor \bar{V}_i b, \; \bar{M}_i, \; \bar{V}_j b, \; \bar{M}_j \right\rfloor \qquad (7)$$

Here, $\bar{V}_i, \bar{M}_i, \bar{V}_j$ and $\bar{M}_j$ are the amplitudes of the nodal line forces V_i, M_i, V_j and M_j, respectively. Now, substituting Eqs. (2) through (7) into Eq. (1) and performing the integrals with respect to the x-coordinate, we shall obtain the following element force-displacement equation by applying the principle of minimum potential energy:

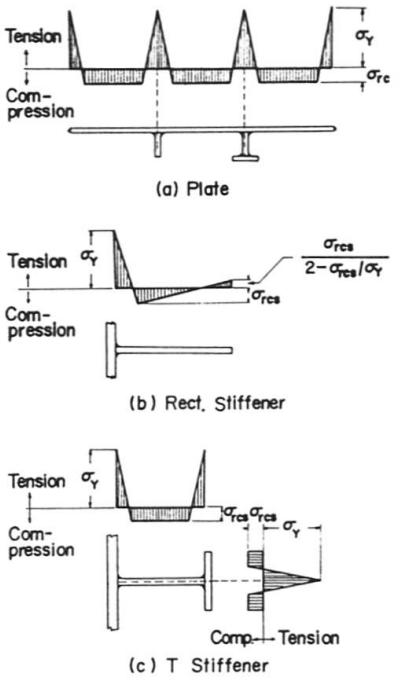

Fig. 2 Assumed Residual Stress Patterns

$$([K] - \lambda^2[K_G])\{\bar{q}\} = \frac{a^2}{D\pi^2 b}\{\bar{Q}\} \ , \quad \lambda = \frac{b}{t}\sqrt{\frac{\sigma_Y}{E}} \tag{8,9}$$

Here, σ_Y is the yield stress of the plate material and $[K]$ and $[K_G]$ denote, respectively, the element stiffness and stability matrices.

Next, we shall consider the potential energy of longitudinal stiffeners. It is arbitrary assumed that a longitudinal stiffener is located along the nodal line i as shown in Fig. 3(a). Owing to the assumption (4) made previously, the rigidities of the stiffener are evaluated at the stage just prior to buckling. Let the y-z coordinate system shown in Fig. 3(a) be a centroidal and principal axis system defined on the unyielded (effective) elastic portions of the stiffener cross-section, and let the effective values of the flexural rigidities about the y and z axes, of the warping torsional rigidity with the shear center and of St. Venant torsional rigidity be denoted by B_y, B_z, C_ω and C_T, respectively. If the cross-sectional distortion is neglected, the total potential energy of the stiffener, Π_s, just after buckling may be given by [2]

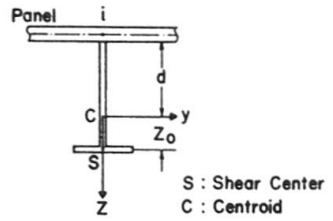

(a) Before Buckling

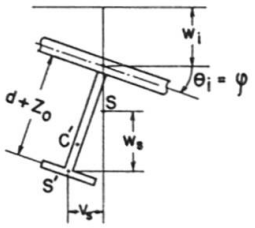

(b) After Buckling

Fig. 3 Deformation of Stiffener

$$\begin{aligned}\Pi_s = \frac{1}{2}\int_o^a \Big[& B_z\left(\frac{d^2v_s}{dx^2}\right)^2 + B_y\left(\frac{d^2w_s}{dx^2}\right)^2 \\ & + C_\omega\left(\frac{d^2\phi}{dx^2}\right)^2 + (C_T + \bar{K})\left(\frac{d\phi}{dx}\right)^2 \\ & - P_s\left\{\left(\frac{dv_s}{dx}\right)^2 + \left(\frac{dw_s}{dx}\right)^2\right\}\Big]dx\end{aligned} \tag{10}$$

where v_s, w_s = displacements of the shear center in the direction of the y and z axes, respectively, ϕ = angle of twist, P_s = axial compressive force acting to the stiffener, and

$$\bar{K} = -\int_{A_s} \sigma_s[(z-z_o)^2 + y^2]dA \tag{11}$$

where σ_s = normal compressive stress on the stiffener cross-section, A_s = area of stiffener cross-section and z_o = z-coordinate of the shear center. Now, if it is assumed that the nodal line i moves only in the direction of z-axis, then the displacements v_s, w_s and ϕ may be expressed approximately in terms of the plate displacements w_i and θ_i as follows (Fig. 3(b)):

$$v_s \cong -(d+z_o)\theta_i \ , \quad w_s \cong w_i \ , \quad \phi = \theta_i \tag{12}$$

where d is the distance between the surface of the plate and the centroid of the stiffener. Upon substitution of Eqs. (12) into Eq. (10), we shall obtain the expression for the potential energy of the stiffener with the plate displacements w_i and θ_i being its variables. Combining this with Eq. (1) leads to the expression for the total potential energy of a strip having a longitudinal stiffener along its nodal line i. As a result, diagonal matrices $[K]_s$ and $[K_G]_s$ expressed by Eqs. (13) are, respectively, superimposed on $[K]$ and $[K_G]$ to incorporate the effects of a longitudinal stiffener located along the nodal line i:

$$[K]_s = \begin{bmatrix} \gamma\bar{B}_y(\frac{\pi}{\alpha})^2 & & \\ & \{\gamma_\omega\bar{C}_\omega + \gamma_z\bar{B}_z(\bar{d}+\bar{z}_o)\}(\frac{\pi}{\alpha})^2 + \gamma_T\bar{C}_T & \\ & & 0 \\ & & 0 \end{bmatrix} \tag{13a}$$

$$[K_G]_s = 12(1-\nu^2) \begin{bmatrix} \bar{P}_s\delta & & \\ & \delta\gamma_p\{\bar{K}_p + \bar{P}_s(\bar{d}^2 - \bar{z}_o^2)\} & \\ & & 0 \\ & & 0 \end{bmatrix} \tag{13b}$$

where α = a/b (aspect ratio). In Eqs. (13), $\gamma, \delta, \gamma_\omega, \gamma_T$ and γ_p are parameters to specify the relative rigidities of the stiffener, which are given by

$$\gamma = \frac{EI_y}{bD} \quad \delta = \frac{A_s}{bt} \quad \gamma_\omega = \frac{EI_\omega}{b^3D} \quad \gamma_z = \frac{EI_z b_s^2}{b^3D} \quad \gamma_T = \frac{GK_T}{bD} \quad \gamma_p = (\frac{b_s}{b})^2 \tag{14}$$

where EI_y, EI_z, EI_ω and GK_T are the constant elastic values of the stiffener rigidities B_y, B_z, C_ω and C_T, respectively. Furthermore, the quantities $\bar{B}_y, \bar{B}_z, \bar{C}_\omega, \bar{C}_T$, $\bar{d}, \bar{z}_o, \bar{P}_s$ and $\bar{K}_p$ in Eqs. (12) are defined by

$$\begin{aligned} \bar{B}_y &= \frac{B_y}{EI_y} \quad \bar{B}_z = \frac{B_z}{EI_z} \quad \bar{C}_\omega = \frac{C_\omega}{EI_\omega} \quad \bar{C}_T = \frac{C_T}{GK_T} \quad \bar{d} = \frac{d}{b_s} \\ \bar{z}_o &= \frac{z_o}{b_s} \quad \bar{P}_s = \frac{P_s}{A_s\sigma_Y} \quad \bar{K}_p = -\frac{\bar{K}}{bD}\frac{1}{12(1-\nu^2)\delta\gamma_p\lambda^2} \end{aligned} \tag{15}$$

These quantities are variable with the magnitude of applied load and, consequently, with the expansion of yielded zones in the stiffener. A special mention is made of evaluating the flexural rigidity EI_y or B_y. As pointed out by Bleich [2], when the stiffeners are welded to one side of a plate, a considerable increase in the flexural rigidity of the stiffeners is observed because of some adjacent zones of the plate taking part in the bending of the deflected stiffeners. Bleich has recommended to include a plate strip having the width 30t as an effective width. In this report, however, an alternative method specified in Refs. [4] and [12] is adopted; the flexural rigidity is computed about an axis parallel to the plate surface at the base of the stiffeners. Assembling the element force-displacement Eqs. (8) combined with Eqs. (13) in consideration of suitable boundary conditions yields the following eigenvalue equation:

$$([\mathbb{K}] - \lambda^2[\mathbb{K}_G])\{\bar{q}\} = 0 \tag{16}$$

where $[\mathbb{K}]$, $[\mathbb{K}_G]$, $\{\bar{q}\}$ are assembled matrices of $[K]$, $[K_G]$ and $\{\bar{q}\}$, respectively. The square root of the minimum eigenvalue determined from Eq. (16) corresponds to the critical width-thickness ratio of the plate.

2.2 Numerical Results and Discussions

Throughout the numerical examples presented in this paper, each subpanel of a stiffened plate was divided into two strip elements, and each strip element was divided into ten segments to calculate the plate stiffnesses.

Shown in Fig. 4 is an example of the computed buckling curves for plates with two stiffeners of flat type. The yield stresses of the plate and the stiffeners are assumed to be equal. The ordinate represents the ratio of average critical stress to the yield stress, σ_{cr}/σ_Y, and the abscissa is the nondimensionalized width-thickness ratio (or the plate parameter) defined by

$$R = \frac{b}{t}\sqrt{\frac{\sigma_Y}{E}\frac{12(1-\nu^2)}{\pi^2 k_o}} \qquad (k_o = 4n^2) \quad (17)$$

where n is the number of subpanels (n = 3 in this case) and k_o is the minimum values of the elastic buckling coefficient of the plates whose stiffeners offer infinitely large flexural resistance but negligible torsional resistance. The aspect ratio α and the relative cross-sectional area δ are fixed, whereas three different values of the relative flexural rigidity γ are considered as multiples of γ_{req} which represents a required relative flexural rigidity of longitudinal stiffeners specified in Ref. [12] (see Appendix). Curves (b) and (c) show, respectively, the buckling curves of the unstiffened plates (i.e., n = 1 and k_o = 4) whose unloading edges are both simply supported, and whose one unloading edge is fixed and the other simply supported. Thus, curve (c) gives the upper bound for the buckling strength of the stiffened plates, whereas curve (b) gives the lower bound so long as the effective flexural rigidity of the stiffeners remains larger than its optimum value γ^* (see Appendix). If the torsional rigidities of the stiffeners are ignored as in the conventional buckling analysis, the three computed buckling curves must coincide with curve (b) in the elastic range (i.e., $\sigma_{cr} < 0.7\sigma_Y$) because their relative flexural rigidities γ are all greater than or equal to their optimum value. Thus it will be understandable that a rather large increase in buckling strength can be expected in the elastic range owing to the torsional resistance of stiffeners. In the range of inelastic buckling the computed buckling curves have rather sharp knee points around $\sigma_{cr}/\sigma_Y = 0.8 \sim 0.9$ regardless of the values of γ, and deviate largely from the upper bound curves. This remarkable reduction in the strength is solely due to the fact that, at these stages of loading, yielding in the stiffeners spreads into their tips so that their effective flexural rigidities B_y are reduced considerably to result in almost zero. This situation is explained in Fig. 5, in which the variation of the effective flexural and torsional rigidities are shown with average critical stress σ_{cr} or the corresponding axial strain ε_{cr} in nondimensional form. It is seen that the effective flexural rigidity B_y becomes almost zero in the range of σ_{cr}/σ_Y above 0.9 when $\sigma_{rcs} = 0.3\sigma_Y$. Figure 6 shows the buckling strength curves of various stiffened plates. It is seen that all curves are quite similar in the region of R between 0.4 and 0.9.

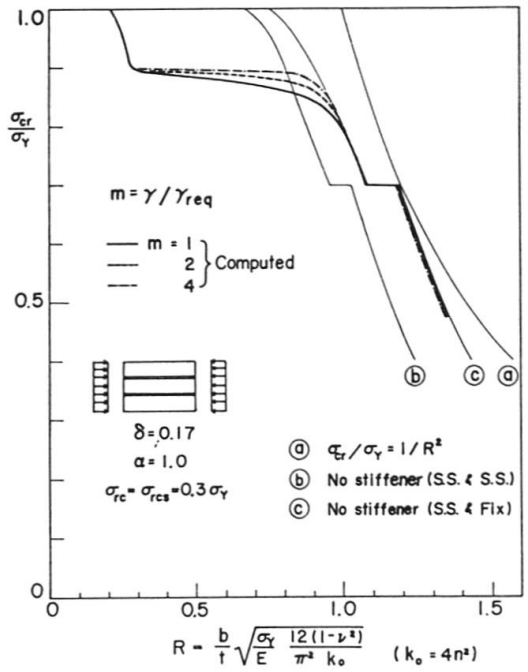

Fig. 4 Buckling Strength Curve (Homogeneous Plate)

Figure 7 shows the buckling strength curves for "hybrid stiffened plates" in which the yield point stress of the stiffener material is higher than that of the plate material. The ordinate and abscissa are nondimensionalized by using a modified yield stress σ'_Y defined by

$$\sigma'_y = \sigma_y \frac{1+(n-1)\delta\sigma_{ys}/\sigma_y}{1+(n-1)\delta} \quad (18)$$

where σ_{ys}, σ_y = yield point stresses of the stiffener and plate materials, respectively. Thus the squash load of a hybrid stiffened plate is given by $\sigma'_Y A$, where A is the total cross-sectional area of the stiffened plate. The stiffener flexural rigidity is assumed to be equal to its optimum value (see Appendix). From the figures it is clearly seen that in all cases the buckling strengths increase with the increase in the yield stress ratio σ_{ys}/σ_y. The test results were taken from the tests made at the University of Tokyo [8]. Comparing the test results, one will realize the superiority of "hybrid stiffened plates".

Next, the buckling strength of plates having tee type stiffeners will be discussed. At first, the variation of the effective flexural rigidity B_y is examined for this type of stiffeners. Figure 8 shows the B_y/EI_y versus $\varepsilon_{cr}/\varepsilon_Y$ curves for three different tee stiffeners. The thickness of the web is assumed to be equal to that of the flange. Compared the curves with those for flat type stiffeners (Fig. 5), one will realize that the reduction of the effective flexural rigidity is much gentler in tee cross-sections than in flat cross-sections. This fact suggests that tee cross-sections will be more favourable than rectangular cross-sections. It is also seen that the curves are not much affected by the ratio of the flange width to the web width, b_{sf}/b_s. The computed buckling curves is shown in Fig. 9. The thicknesses of the stiffener flange and web are assumed to be equal, and the b_{sf}/b_s ratios is 0.2. As might be expected from the foregoing discussion, the strength reductions due to yielding in the stiffeners are rather

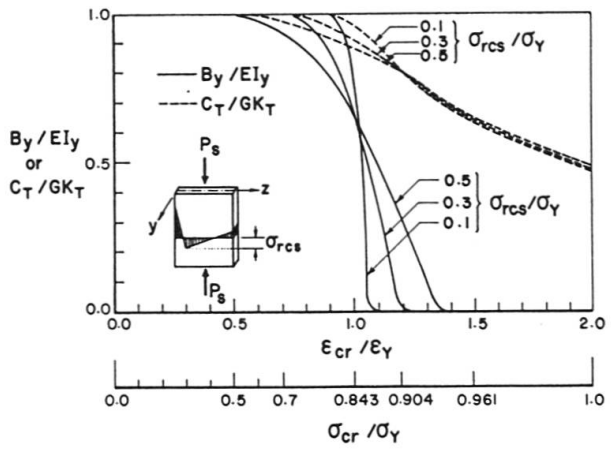

Fig. 5 Variation of Flexural and Torsional Rigidities of Flat-type Stiffener

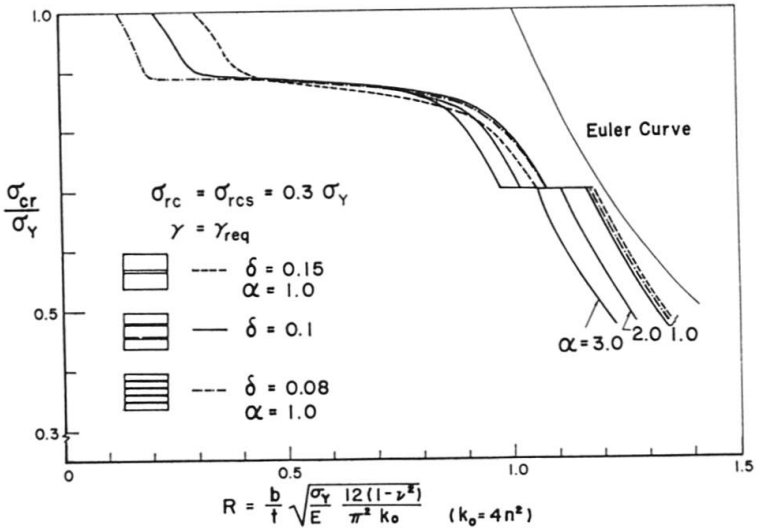

Fig. 6 Buckling Strength Curves of Various Plates (Homogeneous Plates)

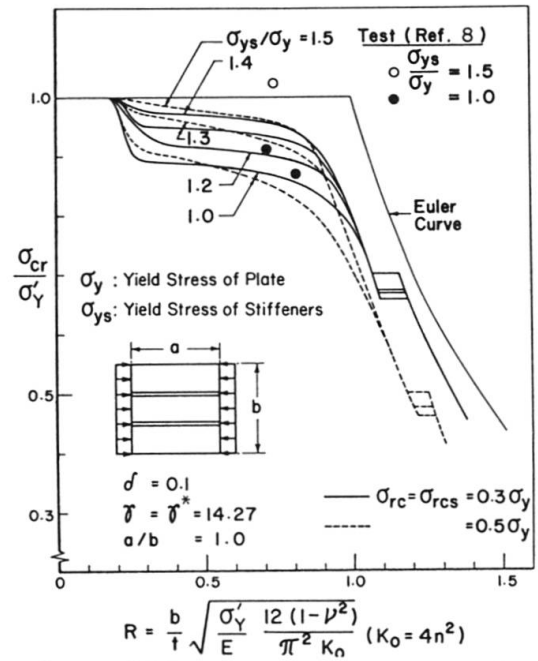

Fig. 7 Buckling Strength Curves of Hybrid Stiffened Plates

gradual in this type of stiffened plates. It is noteworthy that increase of the value of γ from γ^* to $2\gamma^*$ results in fairly large increase in the strength and that, when R is equal to 0.6, the buckling strength reaches as much as 98 percent of the fully yielding strength.

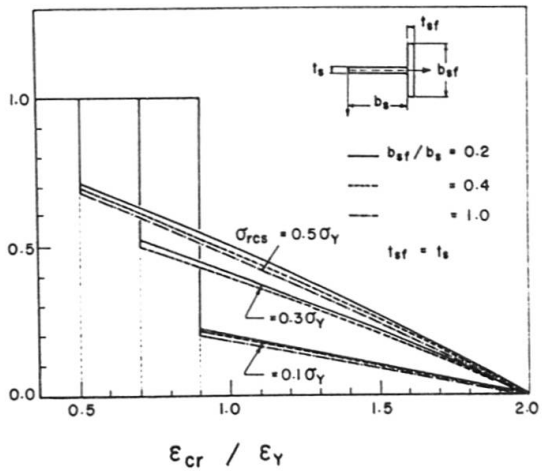

Fig. 8 Variation of Flexural Rigidity of Tee Stiffener

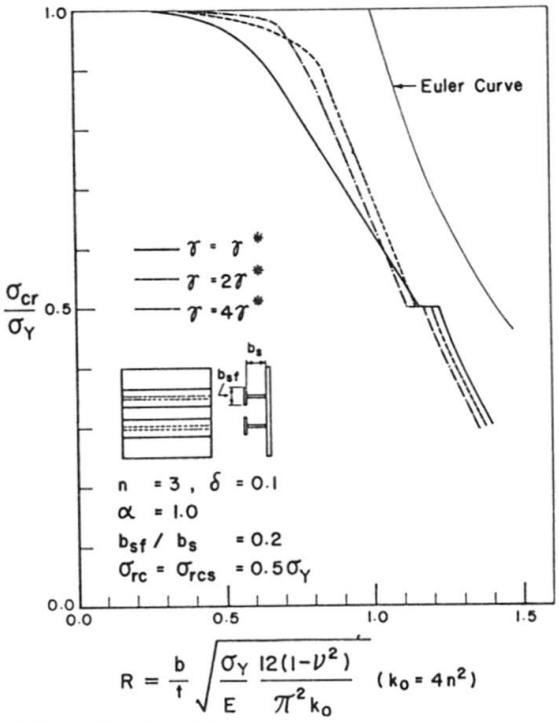

Fig. 9 Buckling Strength Curves of Plates with Tee Stiffeners

3. TEST

3.1 Description of Test

The test were performed under simply supported conditions along the four edges of the panels. Flat type stiffeners of the same grade of steel as the plate panel were used throughout the tests. Table 1 shows a summary of failure test specimens. Each stiffener was welded to the main plate material using 7 mm continuous fillet weld (single pass). In order to simulate the welding conditions in actual box section members, welding bead was provided along each unloading edge of test specimens. Besides the failure tests, six specimens were fabricated for measuring residual stress distributions in a similar way as the failure test specimens. The nominal dimensions are listed in Table 2. In order to satisfy the simply supported conditions along the unloading edges, a special rig was carefully designed and used for the tests as shown in Fig. 10. The channel shaped rigs are clamped to the unloading edges with 75 mm spacing along their direction. Each of the rig is connected to a steel pipe of 22 mm diameter via a universal joint, and the far end of the pipe is fixed to the rigid wall through another universal joint. The set of steel pipes prevent the plate deflections along the unloading edges, while the plate is free to rotate along the same edges owing to the action of the universal joint rigs. Top and bottom ends of the plate and the stiffeners were carefully milled flat in order to obtain the close surface contact with the loading plates. Between the loading plate and the top spreader beams, which are carried on the overhead of the testing machine, a set of semi-circular roller bearings are inserted side by side along the loading edges to represent the simply supported end condition. Each specimen was set in position so that the axial line load was applied through the centroidal axis of the end cross-sections of the specimen. Residual stress measurements were made by the method of sectioning [10] using a 100 mm contact type mechanical strain gage.

3.2 Test Results and Discussions

Material tests were carried out with two tension coupon specimens for each steel plate. The results are shown in Table 3. Figure 11 shows a result of the residual stress measurements together with the assumed residual stress patterns

presented in Fig. 2. The correlation seems to be reasonably good. Two of the other test results are shown in Fig. 12. The values of σ_{rc} and σ_{rcs} given in each figure indicate average values of maximum compressive residual stress measured in each subpanel and in each stiffener, respectively. The measured values of σ_{rc} and σ_{rcs} are summarized in Table 4, together with values predicted by the formulas in Ref. [14]. Rather high residual compressive stresses have been observed throughout the tests. As expected, the observed value of σ_{rc} becomes higher as the width-thickness ratio (b/nt) of panels becomes smaller, and for the R-5 specimen that has the smallest value of b/nt among the test specimens the residual compressive stress σ_{rc} reaches as high as 70 percent of the yield stress. On the other hand, the residual stress σ_{rcs} in the stiffeners remains in the range of 35 to 60 percent of the yield stress and seems to have little correlation with the width-thickness ratios of panels as well as of stiffeners. Comparison between the measured and predicted values of residual stress has shown that the prediction always gives somewhat overestimated values.

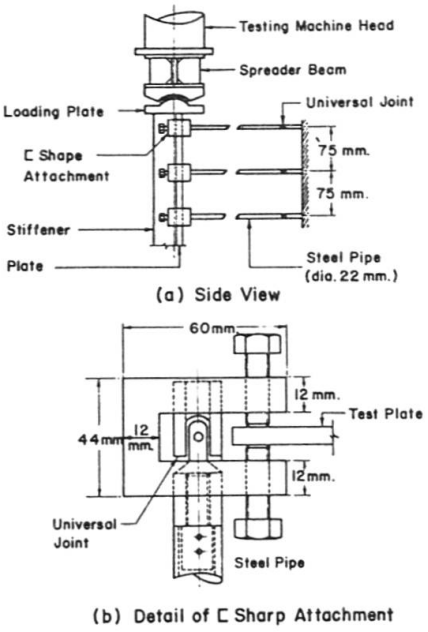

Fig. 10 Test Rigs

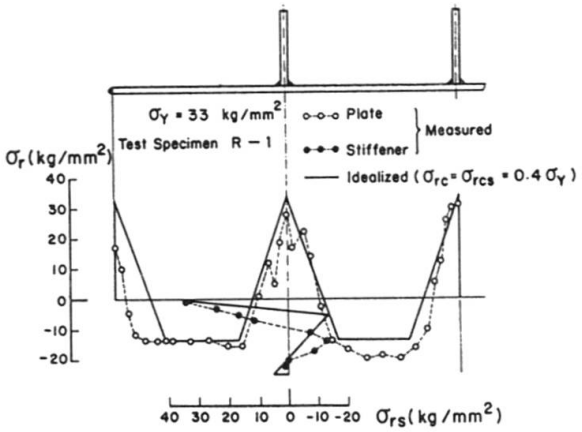

Fig. 11 Measured and Idealized Residual Stress Patterns

The failure test results are summarized in Table 5, where the maximum stress σ_{max} for each specimen is obtained by dividing the maximum load P_{max} by the cross-sectional area A. The failure mode numbers in the last column correspond to the following failure mechanisms:

1) Local torsional buckling of the stiffeners.

2a) Out-of-plane deflection due to overall buckling towards the unstiffened face of panel.

2b) Out-of-plane deflection due to overall buckling towards the stiffened face of panel.

Failure mode 1 has been observed for specimens with relatively high b_s/t_s ratios, whereas most of the other specimens have been terminated by failure mode 2b. Shown in Figs. 13 and 14, are comparisons of the experimental maximum stresses σ_{max}/σ_Y with typical computed buckling stress curves presented before. The test results for specimens with $\gamma \cong \gamma_{req}$ are plotted in Fig. 13 and the others in Fig. 14. Bearing in mind that, as stated before, the buckling curves are not much dependent on the dimensions of the plates in the region of R under consideration, the reference curves shown in the figures may be considered to give fairly accurate predictions for the strengths of all test specimens. From Fig. 13 it is seen that the buckling curves are generally in good agreement with the

Table 1 Dimensions of Compression Test Specimens

Specimen No.	Steel	n	a (mm)	b (mm)	t (mm)	b_s (mm)	t_s (mm)	b/nt	b_s/t_s	γ	γ_{req}	γ/γ_{req}	δ	a/b
B-1-1	SM50A	4	921	766	6.13	60.0	5.83	31.2	10.3	26.1	26.9	0.97	0.074	1.20
B-1-1r			916	767	5.73	60.3	6.03	33.5	10.0	33.6	29.2	1.15	0.083	1.20
B-1-2			920	765	6.00	72.3	6.00	31.9	12.1	50.3	30.1	1.67	0.095	1.20
B-2-1			803	670	5.87	52.8	5.80	28.5	9.1	23.1	22.5	1.03	0.078	1.20
B-2-4			803	670	6.02	83.4	7.95	27.8	10.5	115.6	27.3	4.25	0.164	1.20
B-3-1			630	526	6.10	41.4	6.00	21.6	6.9	13.1	12.2	1.07	0.077	1.20
C-1-1	SS41	5	1436	1200	5.85	82.9	5.77	41.0	14.4	50.1	37.4	1.34	0.068	1.20
C-1-2			1434	1197	5.80	105.6	5.70	41.3	18.5	105.3	40.1	2.62	0.087	1.20
C-1-4			1436	1198	5.93	126.8	8.40	40.4	15.3	251.1	49.2	5.1	0.150	1.20
C-2-1			1291	1076	5.87	75.7	5.90	36.7	12.8	43.1	37.8	1.14	0.071	1.20
C-2-2			1291	1076	5.88	94.4	5.82	36.6	16.2	82.0	40.1	2.04	0.087	1.20
C-2-4			1293	1074	5.84	114.9	8.30	36.8	13.8	215.6	49.6	4.36	0.152	1.20
C-3-1			1148	958	5.93	65.0	6.04	32.3	10.8	30.4	29.1	1.04	0.069	1.20
C-3-2			1147	959	6.00	85.0	5.85	32.0	14.5	63.5	30.0	2.11	0.086	1.20
C-3-4			1152	960	6.00	102.0	8.00	32.0	12.8	150.0	35.8	4.19	0.142	1.20
C-4-1			1003	840	5.87	57.0	6.03	28.6	9.5	24.1	22.2	1.09	0.070	1.20
C-4-2			1004	838	5.73	75.0	5.86	29.3	12.8	57.4	25.1	2.29	0.092	1.20
C-5-1			895	749	5.92	51.9	6.00	25.3	8.7	19.8	17.2	1.15	0.070	1.20
C-6-1			2393	1194	5.99	110.0	8.24	39.9	13.3	156.6	126	1.24	0.127	2.00
C-7-1			2160	1073	6.06	98.5	8.39	35.4	11.7	123.0	115	1.07	0.127	2.01
C-8-1			1912	957	5.98	88.3	8.92	32.0	9.9	109.9	93.7	1.17	0.128	2.00
D-1-1	SS41	6	1192	969	4.66	59.5	6.03	34.7	9.9	47.4	43.9	1.08	0.079	1.23
D-1-2			1200	972	4.50	76.0	5.85	36.0	15.2	106.2	52.0	2.04	0.102	1.23
D-1-3			1190	965	4.68	89.0	5.95	34.4	15.0	155.3	50.0	3.16	0.117	1.23
D-2-1			1022	862	4.71	52.0	6.06	30.5	8.6	34.7	33.6	1.03	0.078	1.19
D-2-3			1028	860	4.55	79.6	5.94	31.5	13.4	135.5	42.4	3.20	0.121	1.20
D-3-1			798	677	4.68	41.6	5.94	24.1	7.0	22.6	20.6	1.10	0.078	1.18

Table 2 Nominal Dimensions of Test Specimens for Residual Stress Measurement

Specimen No.	Steel	n	a (mm)	b (mm)	t (mm)	b_s (mm)	t_s (mm)	b/nt	b_s/t_s
R – 1	SM50A	4	1400	1152	9	126	9	32	14
R – 2			1400	1152	9	90	9	32	10
R – 3			1400	1152	9	54	9	32	6
R – 4			1200	1008	9	90	9	28	10
R – 5			1000	792	9	90	9	22	10
R – 6			1100	864	6	60	6	36	10

test results. Some test results fall below the prediction curves. This may be due to the effects of initial deflections, or more possibly due to higher residual stresses than the assumed ones. The test results in Fig. 14 show more scattered results. On examination of the test specimens whose maximum stresses fall below the prediction curves, it will be found out that the width-thickness ratios b_s/t_s of their stiffeners are comparatively large (the figures in the parentheses beside the test points indicate the b_s/t_s ratios). The critical b_s/t_s ratio for a flat stiffener, such that local buckling would not occur before

the attainment of yield stress, may be determined from Eq. (17.22) of Ref. [16]. If the stiffener is assumed to be simply supported along the welded edge (i.e., the buckling coefficient k = 0.425), the critical width-thickness ratio becomes approximately 13.0 for SS41 (σ_Y = 2,400 kg/cm^2) and 12.0 for SM50 (σ_Y = 3,200 kg/cm^2). These might be a little conservative figures because no edge restraint by the plate panel is taken into account. Nevertheless, considering the fact that most of the test results for high b_s/t_s ratios exceeding the critical values fall below the predicted buckling strengths and that the test specimens with lower b_s/t_s ratios tend to give higher strengths when the width-thickness ratios of the panels are nearly identical, the above figures of the critical b_s/t_s ratio may be adopted as a requirement in the design of flat type stiffeners. If the test results for high b_s/t_s ratios exceeding the critical values are excluded, most of the experimental maximum loads exceed the predicted strengths and, when the width-thickness ratio of the panel R is approximately 0.6, the fully yielded strength

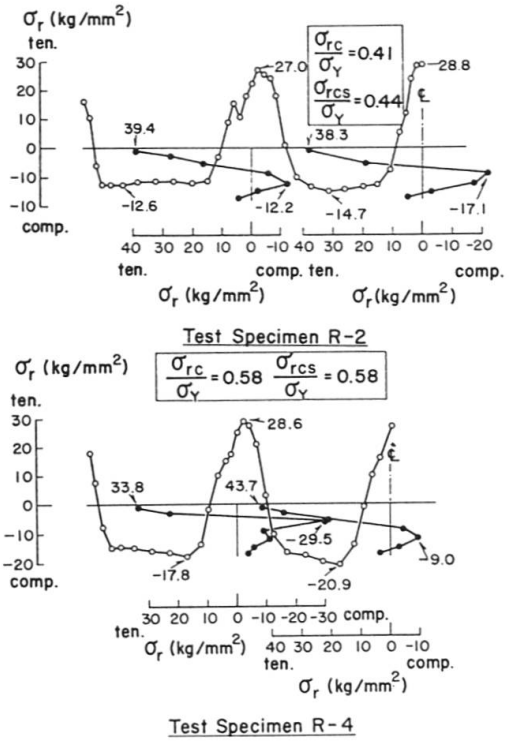

Fig. 12 Measured Residual Stress Distributions

Table 3 Tension Coupon Test Results

Material (Nominal Thickness)	Thickness (mm)	Yield Stress (kg/cm^2)	Modulus of Elasticity (kg/cm^2)	Ultimate Stress (kg/cm^2)
SS41 (6 mm)	5.70	2740	2.13 x 10^6	4340
SS41 (8 mm)	8.25	2780	2.13 x 10^6	4590
SM50A(6 mm)	6.00	3630	2.10 x 10^6	5670
SM50A(9 mm)	9.10	3320	2.14 x 10^6	5230

Table 4 Comparison of Measured and Predicted Values of Maximum Compressive Residual Stresses

Specimen No.	Yield Stress	$\frac{b}{nt}$	R	$\frac{b_s}{t_s}$	Measured		Predicted
					σ_{rc}/σ_Y	σ_{rcs}/σ_Y	$\sigma_{rc}/\sigma_Y = \sigma_{rcs}/\sigma_Y$
R - 1	3300 kg/cm^2	32	0.667	14	0.50	0.39	0.56
R - 2		32	0.667	10	0.41	0.44	0.62
R - 3		32	0.667	6	0.35	0.35	0.67
R - 4		28	0.584	10	0.58	0.58	0.69
R - 5		22	0.459	10	0.71	0.44	0.82

has been obtained. The discrepancy between the test and the theory is not apparent, however, one possible reason would be the effect of post buckling strength of test plates. In our present test program attention has been focused on the strength of stiffened plates with low width-thickness ratios and, therefore, information has been lacking on the applicability of the theory to wider range of stiffened plates. Here, we shall gather the test data obtained in other institutions mainly in Japan and compare them with the theoretical predictions. Figure 15 shows such a comparison, where the experimental maximum stresses obtained from tests in five institutions [5,8,9, 11,13] in addition to our university are plotted to compare typical buckling curves. It is noted that the test results for high b_s/t_s ratios exceeding the aforementioned critical width-thickness ratio are excluded from plotting in the figure. Each of the test specimens quoted was made of structural carbon steel or high strength low alloy steel and was tested as an isolated plate panel or as a square box section. The stiffener cross-section used was mostly flat type, but some of the test specimens in Ref. [5] have longitudinal stiffeners of bulb flat type. It is surprising that even the test results in the range of large width-thickness ratios show a tendency to agree well with the theoretical buckling curves. It seems that in the range of R beyond 0.8 the strengths tend not to depend on the relative flexural rigidity γ provided that it is greater than the optimum value.

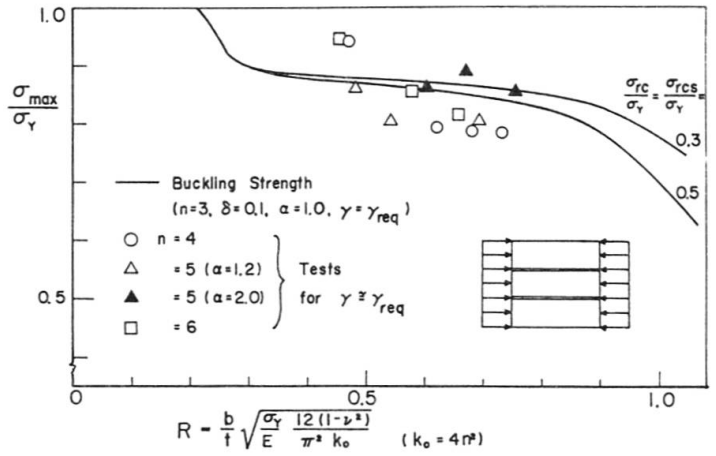

Fig. 13 Comparison of Test and Theory ($\gamma = \gamma_{reg}$)

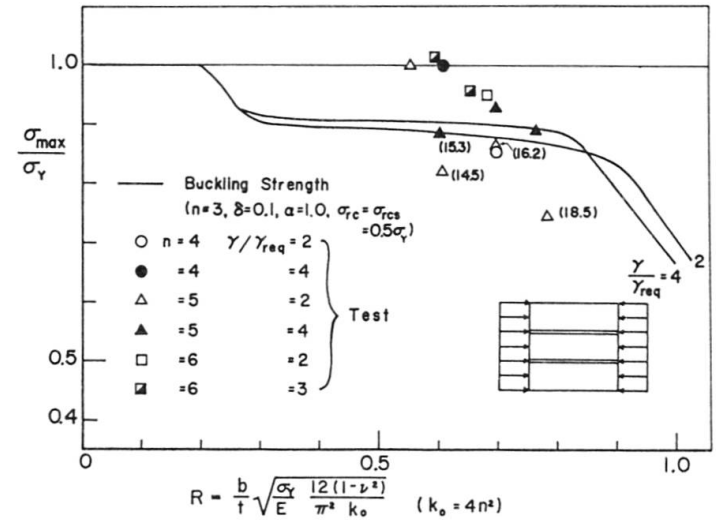

Fig. 14 Comparison of Test and Theory (γ = 2 or 4 γ_{reg})

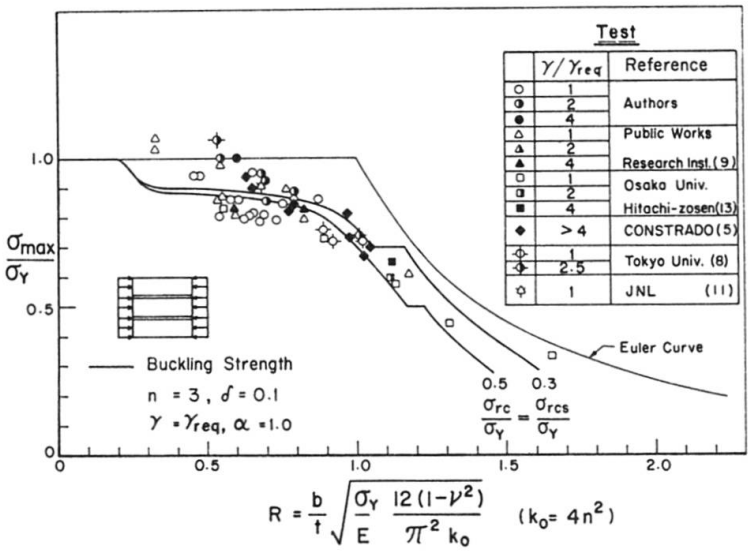

Fig. 15 Comparison of Test and Theory

Table 5 Summary of Compression Test Results

Test Specimen No.	A (cm^2)	P_{max} (tons)	σ_{max} (kg/cm^2)	σ_y (kg/cm^2)	σ_{max}/σ_y	R	Failure Mode
B-1-1	57.44	166.0	2890		0.785	0.682	2-b
B-1-1r	54.86	159.8	2904		0.789	0.733	2-b
B-1-2	58.91	185.0	3140	3630	0.853	0.698	1&2-a
B-2-1	48.51	141.8	2923		0.794	0.623	2-a
B-2-4	60.22	222.2	3690		1.003	0.608	1&2-a
B-3-1	39.54	137.0	3465		0.941	0.472	2-b
C-1-1	89.33	138.6	1552		...	...	**
C-1-2	93.50	192.3	2057		0.746	0.784	1
C-1-4	113.60	278.5	2450		0.889	0.766	2-b
C-2-1	81.02	179.3	2213		0.803	0.695	2-b
C-2-2	83.25	200.3	2350		0.853	0.694	1
C-2-4	100.87	257.7	2550		0.927	0.697	1
C-3-1	72.51	137.5	1896		...	...	**
C-3-2	77.43	175.0	2260		0.820	0.606	2-b
C-3-4	90.24	220.0	2438	2740	0.885	0.607	2-b
C-4-1	63.05	140.0	2220		0.806	0.543	2-a
C-4-2	65.58	181.5	2768		1.004	0.554	2-b
C-5-1	56.81	134.9	2375		0.862	0.481	2-b
C-6-1	107.77	251.0	2329		0.845	0.756	2-b
C-7-1	98.07	240.5	2452		0.890	0.671	2-b
C-8-1	86.49	205.6	2377		0.862	0.607	2-b
D-1-1	63.09	141.5	2243		0.814	0.657	2-b
D-1-2	65.97	172.2	2610		0.947	0.683	2-b
D-1-3	71.64	138.5	2631	2760	0.955	0.652	1
D-2-1	56.33	132.9	2359		0.856	0.578	2-a
D-2-3	62.77	175.2	2791		1.013	0.597	1
D-3-1	44.06	114.8	2606		0.946	0.457	2-b

4. CONCLUSIONS

A theoretical and experimental investigation has been presented on the strength of longitudinally stiffened steel plates in edge compression. From the numerical study it has been found that partial yielding in the flat stiffeners due to applied stress plus residual stresses reduces considerably the buckling strength of stiffened plates. In order to avoid a great reduction of the strength, a higher strength steel is recommended to use for the flat stiffeners than for the plate, "hybrid stiffened plate". The superiority of the "hybrid stiffened plates" has been confirmed theoretically and experimentally. In the case of plates stiffened by tee type stiffeners, the strength reductions due to partial yielding in the stiffeners are found to be rather gradual and, therefore, this type of stiffeners seems to be preferable to flat type stiffeners. In the experimental study, a total of twenty-seven failure tests were made on stiffened plates with three to five flat type stiffeners. Residual stress measurements

were also made on six specimens. The measured residual stress distributions have generally agreed with the assumed residual patterns show in Fig. 3. The experimental maximum strengths are generally in good agreement with the theoretical predictions, however, the predictions tend to slightly underestimate the strengths of the test plates having relatively rigid stiffeners.

REFERENCES

1. Bijlaard, P.P., "Theory of the Plastic Stability of Thin Plates", IABSE Publications, Zurich, Vol. 6, 1940.
2. Bleich, F., "Buckling Strength of Metal Structures", McGraw-Hill, New York, 1952.
3. Cheung, Y.K., "Finite Strip Method of Analysis of Elastic Slabs", Proc. ASCE, Vol. 94, EM6, 1968.
4. DIN 4114, Blatt 2, "Stahlbau, Stabilitätfalle (Knichung, Kippung, Beulung), Berechnungsgrundlagen, Richtlinien", Feb., 1953.
5. Dorman, A.P., Dwight, J.B., "Tests on Stiffened Compression Plates and Plate Panels", International Conference on Steel Box Girder Bridges, ICE, Feb., 1973.
6. ECCS, "Manual on the Stability of Steel Structures", 1976.
7. Fukumoto, Y., Usami, T. and Okamoto, Y., "Ultimate Compressive Strength of Stiffened Plates", Proc. ASCE Specialty Conference on Metal Bridge, St. Louis, Mo., U.S.A., Nov., 1974.
8. Hasegawa, A., Nagahama, M. and Nishino, F., "Buckling Strength of Stiffened Plates under Compression", Proc. JSCE, No. 236, Apr., 1975 (in Japanese).
9. Fujiwara, M., Hara, M. and Amamiya, A., "Experimental Study on Ultimate Compressive Strength of Stiffened Plates", Proc. 30th JSCE Annual Meeting, 1975 (in Japanese).
10. Huber, A.W. and Beedle, L.S., "Residual Stress and the Compressive Strength of Steel", Welding Journal, Vol. 33, Dec., 1954.
11. Ito, F. and Tajima, I., "Compression Test of Welded Short Columns Built-up with Stiffened High Tensile Strength Steel Plates", Railway Technical Research Report No. 313, Railway Technical Research Institute, Japanese National Railway, 1962 (in Japanese).
12. Japan Road Associations, "Specifications for Highway Bridges", 1972.
13. Komatsu, S., Ushio, M. and Kitada, T., "An Experimental Study on Ultimate Strength of Stiffened Plates in Compression", Proc. JSCE, No. 254, Oct., 1976 (in Japanese).
14. Merrison Committee, "Inquiry into the Basis of Design and Method of Erection of Steel Box Girder Bridges, Appendix 1 (Interim Design and Workmanship Rules)", Her Majesty's Stationery Office, London, 1973.
15. Nishino, F., "Buckling Strength of Columns and Their Component Plates", Ph.D. Dissertation, Lehigh University, 1964.
16. Ostapenko, A., "Local Buckling", in "Structural Steel Design", Tall, L., ed., The Ronald Press, New York, 1964.
17. Przemieniecki, J.S., "Matrix Analysis of Local Instability in Plates, Stiffened Panels and Columns", International Journal for Numerical Methods in Engineering, Vol. 5, 1972.
18. Timoshenko, S.P. and Gere, J.M., "Theory of Elastic Stability", McGraw-Hill, New York, 1961.
19. Usami, T., "Elastic and Inelastic Buckling Strength of Stiffened Plates in Compression", Proc. JSCE, No. 228, Aug., 1974 (in Japanese).

APPENDIX

The expression for γ_{req} specified in Ref. [12] is, with a slight modification, given as follows:

$$\gamma_{req} = 4\alpha^2 n\left(\frac{R}{R_{cr}}\right)^2(1+n\delta) - \frac{(\alpha^2+1)^2}{n} \quad \text{(when } R \leq R_{cr} \text{ and } \alpha \leq \alpha_o\text{)} \qquad \text{(A.1)}$$

$$\gamma_{req} = \frac{1}{n}(\alpha_o^4-1) \quad \text{(when } R \leq R_{cr} \text{ and } \alpha \geq \alpha_o\text{)} \qquad \text{(A.2)}$$

where

$$\alpha_o = \sqrt{2n^2\left(\frac{R}{R_{cr}}\right)^2(1+n\delta)-1} \qquad \text{(A.3)}$$

Here, R_{cr} is a value of R at which an unstiffened plate (i.e., n = 1) is supposed to reach its squash load. In Ref. [12], this value is assumed to be 0.7. Note that Eqs. (A.1) to (A.3) are valid when R is less than or equal to R_{cr}. When R is larger than R_{cr}, the same expressions but with $R = R_{cr}$ must be used. The expressions for γ_{req} with $R = R_{cr}$, which is denoted by γ^*, provide very close values to the optimum relative stiffener rigidity specified in DIN4114 [4].